

The X-Ray origin of Herbig AeBe Systems: New Insights

Murad Hamidouche¹, Shiya Wang, Leslie W. Looney

Astronomy Department, University of Illinois, Urbana, IL 61801

mhamidouche@sofia.usra.edu

ABSTRACT

We present a statistical study of the X-Ray emission toward 22 Herbig AeBe stars using the Chandra archive. We probe the origin of the X-Rays toward Herbig stars: are they intrinsic? This question is addressed by correlations between the physical stellar properties and the X-Ray emission. There is a weak correlation between the continuum radio emission at $\lambda=3.6$ cm and L_X , which suggests that the X-Ray emission depends upon the source. On the other hand, no correlation was found with the stellar rotational period, but that only excludes solar-like magnetic activity as the origin of the X-Rays. Most importantly, the X-Ray luminosity of Herbig AeBe stars have a different distribution than T Tauri stars, suggesting X-Ray emission from an unseen late type star companion can be ruled out with an 80% confidence level. This implies that the Herbig AeBe stars must have magnetic activity. In addition, we report the observation of five sources for the first time, three detections.

Subject headings: stars: Herbig AeBe, pre-main-sequence - X-Rays: stars - methods: statistical - radiation mechanisms: thermal

1. Introduction

Herbig AeBe stars (HAEBE) are young intermediate mass stars, ranging roughly from 2 to 20 M_\odot of spectral type A, B and early F (Herbig 1960). They are considered the more massive counterparts of T Tauri stars (TTS). The study of HAEBE disks has attracted particular interest in investigating their formation and evolution into planetary systems. Unfortunately, their pre-main-sequence (PMS) evolution is more difficult to study with as

¹New address: Stratospheric Observatory for Infrared Astronomy, NASA Ames Research Center, MS 211-3, Moffett Field, CA 94035

much detail as TTS, as they are less abundant and evolve faster; the formation and evolution processes are presumably accelerated and more embedded. The existence of circumstellar disks in HAEBE systems were confirmed with interferometric millimeter observations (e.g. Mannings & Sargent 1997), and more recent results have resolved these disks (e.g. Hamidouche et al. 2006). Fuente et al. (2003) have reported the first evidence of a disk around the more massive Herbig Be stars. The detection of these disks is relevant in probing the X-Ray origin in HAEBE systems. In fact, numerous authors have already suggested star-disk magnetic interactions may generate the X-Rays (Montmerle et al. 2000).

Although X-Ray detection toward HAEBE stars has become quite common (e.g. Hamaguchi et al. 2005; Stelzer et al. 2006), its origin is more difficult to explain than the X-Ray detection of lower mass TTS. The later-type TTSs are also routinely observed in the X-Ray. The process usually invoked to explain their X-Ray origin is solar-type coronal loops in the 1-10 keV band (Feigelson et al. 2007), while in some active protostars, larger magnetic structures can possibly connect the stellar photosphere and the circumstellar accreting disk (Montmerle et al. 2000; Feigelson et al. 2007). Using the Chandra Orion Ultradeep Project, COUP (Getman et al. 2005a), and the XMM-Newton Extended Survey of the Taurus Molecular Cloud, XEST (Güdel 2007), several studies have shown that TTS X-Rays are mostly due to coronal emission and not to accretion emission, which only has a minor effect in the soft < 1 keV regime (e.g. Preibisch 2007; Güdel 2007). Nevertheless, accreting stars were found to have a lower X-Ray activity than non-accreting sources. The accreting material cools down the corona hot plasma. Therefore, the cool plasma generates very soft X-Rays hardly detectable with Chandra and XMM-Newton (Preibisch 2007).

Numerous surveys of X-Ray emission toward HAEBE stars have been done: Stelzer et al. (2006) have reported a fraction of ~ 76 % from a sample of 17 sources using Chandra, including emission from known companions; Hamaguchi et al. (2005) have detected 31% from a sample of 35 sources using ASCA; Zinnecker & Preibisch (1994) have detected 52% from a sample of 21 sources using ROSAT; and Damiani et al. (1994) have detected 35% from a sample of 31 sources using Einstein.

In this paper, we report on a sample of 22 sources using the Chandra archive, 17 sources from Stelzer et al. (2006) and 5 new sources. With these data, we compare the X-Ray emission to the stellar properties in order to look for possible correlations; hence, whether the X-Rays are intrinsic to the Herbig stars or not.

2. Data sample and Observations

We have correlated the Chandra archive with the HAEBE stars catalogs of: Mora et al. (2001), Natta et al. (2000), Thé et al. (1994), and Hillenbrand et al. (1992). We chose the sources of spectral types earlier than F5. This provides a sample to probe and compare the X-Rays of both the coolest Herbig Ae (late B, A and early F) stars and the Herbig Be (early/mid B) stars (e.g. Natta et al. 2000). Data mining the Chandra’s public archive for observed sources allowed us to make a list of 22 HAEBE observations, whether they were serendipitous observations or not. In fact, there are 13 sources that were not observed as the main target, but were in the field of view during other observations. The list of sources with known stellar parameters is given in Table 1.

Fortuitously, our sample includes HAEBE sources of different spectral types, which will provide a better analysis of the X-Ray properties of HAEBE stars. Our sample includes stars of masses ranging between $\sim 2\text{-}26 M_{\odot}$ of different ages between $10^6\text{-}10^7$ years (van den Ancker et al. 1998, 2000).

Table 2 summarizes the Chandra observations. The observations are obtained with the ACIS (Advanced CCD Imaging Spectrometer) detector within Chandra’s band 0.5 to 10 keV. Although many of our sources were reported in Stelzer et al. (2006), the fact that we have 5 addition sources, lead us to re-analyze all of them in order to be consistent. In addition, our detection criteria is more focused on the removal of companion emission (see HD 150193 in §3.1). The Chandra data analysis software CIAO¹ version 3.1 and the X-ray spectral fitting package XSPEC version 11.3 are used for our data reduction and analysis. We obtained the Event 2 level processed data from Chandra Archives. We extract the background lightcurve and use ChIPS to exclude the time periods of high background by removing spikes on the background lightcurve. These processes give the good time interval. The event files with applied good time interval are then used to detect point sources and further extract spectra of these sources.

The WAVDETECT was used to detect point sources within a 50×50 pixel area centered on the source IR/optical position. This algorithm uses Mexican Hat wavelet functions to correlate the images and identify source regions with large positive correlation. We generate regions centered at the detected peak emission within a 3σ ellipse, including 90% of the point spread function (PSF) at 1.497 KeV. With detected point sources, we use Sherpa to plot the radial profile to look for any possible signatures of extra emission that may be due

¹The Chandra Interactive Analysis of Observations (CIAO) software package can be found at: <http://asc.harvard.edu/ciao/>

to companions.

3. Results and discussions

3.1. X-Ray detections

Count rates are estimated within a circular or elliptical region, depending on the source geometry, around the optical position of the source after removing the background. The background is estimated in a different region of the image map and normalized by the surface area of the source region. Our criteria for the detection was based on the signal-to-noise ratio (S/N), S/N higher than ≈ 3 . The count rate was estimated in the “broad” band (0.5-8 keV), including both soft and hard X-Rays. The sources with low S/N were classified as non-detections.

The number of detected sources is 14, out of 22 sources; 8 of the detected sources were serendipitous observations of Chandra, 3 of which had not yet been reported. Table 3 summarizes all the sources and their corresponding X-Ray luminosity. The upper limits were estimated at a 90% confidence level using the Bayesian method (Kraft et al. 1991). The deduced percentage of HAEBE stars detected $\simeq 64\%$ (see Table 3), compared to 76% from Stelzer et al. (2006). Out of the 5 Herbig Be stars, earlier than B6, 3 were detected (60%), and out of the 17 Herbig Ae stars, 11 were detected (65%).

For the 8 brightest detected sources, the flux density was derived by fitting thermal plasma models based on MEKAL² emissivities (Kaastra & Mewe 2000) (Table 4). The flux density, gas column density N_{H_2} , and the gas temperature kT are then derived from this spectral analysis. Extrapolating linearly the flux density values of the 8 brightest sources against the count rates allows an estimation of the flux density for the other 6 sources, which have lower count rates. N_{H_2} from the spectra fitting could be used to correct our flux from the absorption of the gas through the line-of-sight. However, we chose not to correct our flux since these N_{H_2} values are not well determined (e.g. Stassun et al. 2004; Feigelson et al. 2002). The X-Ray luminosity (L_X) were then computed for each source by multiplying the total flux density in the entire band 0.5-8 keV by $4\pi d^2$, where d is the distance of the source (Table 1). In addition to the count rate uncertainties, we consider distance uncertainties to estimate L_X uncertainties. If distance uncertainties are not presented in the literature, we use a 20% uncertainty.

²Mekal = Mewe-Kaastra-Liedahl thermal plasma (1995); <http://cxc.harvard.edu/ciao/ahelp/xs.html>

We can compare our results to those of Stelzer et al. (2006). The deduced $\text{Log } L_X$ are consistent within the uncertainties. However, AK Sco shows a very low count-rate below our detection criteria; we do not consider it as detected. We have also detected X-Ray emission toward HD 150193, but it is offset by $\simeq 2.5''$ from its optical position (cf. Stelzer et al. 2006). These sources were both considered detected by Stelzer et al. (2006).

In addition, this is the first study where Chandra observations toward the additional five sources (underlined in Table 3) are reported (Figure 1). From these five sources, we detected V361 Ori, AB Aur, and V372 Ori, and did not detect LP Ori and MR Ori. Using ASCA, Hamaguchi et al. (2005) also did not detect LP Ori or MR Ori. In the ROSAT survey, Zinnecker & Preibisch (1994) detected AB Aur with a slightly higher $\text{Log } L_X = 29.5$ ergs/sec, while it was not detected by Hamaguchi et al. (2005) and Damiani et al. (1994) using Einstein. V372 Ori was detected by Gagne et al. (1995) in a ROSAT survey, $\text{Log } L_X = 30.3$ ergs/sec. These results are consistent with our detections; however, our L_X are slightly lower since we did not correct for absorption. This is the first detection of V361 Ori.

3.2. X-Ray relations to stellar properties

If the X-ray emission is intrinsic to the stellar systems, there may be some correlation between the star and the X-Ray emission. We have performed Kendall's τ -tests, including the upper limits data (non-detections), as implemented in the ASURV package (Isobe et al. 1986). We compare first the stellar bolometric luminosity with the X-Ray luminosity L_X . We find a mean ratio $\text{Log } (L_X/L_{bol}) = -5.62 \pm 1.18$ for the detected sources (Table 3). This ratio is consistent with the recent values found toward HAEBE stars (e.g. Skinner et al. 2004). Figure 2 (*top*) shows L_X , for detected sources and upper limits for the undetected ones, versus L_{bol} . Most points are between the two lines corresponding to the TTS ratio -3.75 (Skinner et al. 2004) and main sequence OB stars ratio -7.0 (Berghoefer et al. 1997). Using the Kendall's τ -test, we found a probability of $P = 0.42$ that a correlation is not present. Interestingly, the test for the surface area ($4\pi r_*^2 = L_{bol}/\sigma T_{eff}^4$) and L_X provides a similar result $P = 0.39$ (Figure 2, *bottom*).

We probe the relations of L_X with the stellar rotation period, $P_{rot} = 2\pi r_*/v_{rot} \sin i$, and the wind velocity v_{wind} , for the sources with known values (Table 1). We did not find a correlation between the luminosity ratio L_X/L_{bol} and the stellar rotational period P_{rot} , Kendall τ -test probability of no correlation $P = 0.44$ (Figure 3). For comparison, late type main-sequence stars are known to have a clear correlation between the luminosity ratio and the stellar rotation period (Pallavicini et al. 1981; Preibisch 2007). On the other hand, they did not use their non-detection limits, so we repeated the Kendall τ -test for only our

detected sources and still did not find a strong correlation, probability of no correlation $P = 0.65$. Therefore, solar-like magnetic dynamo mechanism can be excluded as the origin of HAEBE X-Ray activity. We used the relation of mass-loss rate and bolometric luminosity for Herbig stars given by (Skinner et al. 1993): $\text{Log } \dot{M} = -9.1 + 0.6 \text{ Log } (L_{bol}/L_{\odot})$ M_{\odot}/year to deduce the wind kinetic luminosity $L_{kin} = 1/2 \dot{M} v_{wind}^2$. Figure 4 shows that L_{kin} is below the dashed line, corresponding to $L_X = L_{kin}$, by about two order of magnitude. In addition, Figure 5 shows that most points are above the maximum temperature, dashed line, that can be generated if all the kinetic energy is converted into thermal bremsstrahlung energy. Although, only three sources have known v_{wind} and do not satisfy this later condition, we can suggest that the wind-shock model does not appear as the origin of the X-Ray emission for these sources. HD 104237 has a wind velocity that may generate part of the X-Rays. Its corresponding point is below the dashed line (Figure 5). Skinner et al. (2004) have suggested a possible existence in this source of a thin convective zone of $\approx 0.9\%$ stellar radius and a magnetic activity, but it may not be strong enough to produce the detected L_X . We can naively suggest that a fraction of the wind kinetic energy can be a complementary process to the stellar coronal magnetic activity to produce the observed X-Rays.

Figure 6 displays L_X versus the radio continuum luminosity at $\lambda = 3.6$ cm, $L_{3.6cm}$. There is a correlation between the two variables. Kendall τ -test's probability of no correlation of only $P = 0.025$, which becomes $P=0.01$ when only the detected sources in both X-Ray and radio are considered in the test. We deduce an almost linear relation between L_X and the stellar radio emission $L_X \propto 10^{11-12} L_{3.6cm} [\text{Hz}]$. Both X-Ray and radio emissions can be related to the stellar magnetic activity at different levels, if assuming that they come from the same star. Similarly, Güdel (2002) reported in his analysis toward active stars with a hot plasma emitting both thermal X-Rays and non-thermal radio radiation. However, we note that our analysis is for Herbig Ae stars only, for which we know $L_{3.6cm}$, and they are known to possibly have a thin convective zone that may generate the X-Rays (e.g. Skinner et al. 2004).

4. X-Ray Emission from Companions?

The X-Ray emission from intermediate mass HAEBE stars (and AB stars) has been a standing puzzle as they are not known to have convective outer layers that generate the magnetic dynamo as in the lower mass TTS (e.g. Feigelson & Montmerle 1999). The most common explanation of the X-Ray origin is from an unresolved lower mass TTS companion (e.g. Zinnecker & Preibisch 1994; Feigelson et al. 2003). However, Chandra can not resolve companions closer than $\simeq 1''$, or ~ 100 -1000 AU for our sources. This is larger than the

typical binary separations, which can be $\sim 0.1''$ (e.g. Baines et al. 2006; Tokovinin et al. 2006).

4.1. Comparison to the Orion Nebula sources

We combine our detected HAEBE stars data with TTS and HAEBE stars observed in the ONC. The Orion observations used here are from the COUP project. COUP has detected more than 1600 X-Ray sources of different spectral types and ages $\sim 10^{4.2} - 10^{7.6}$ years, a similar age range to our sources. We select COUP stars that have known spectral types. Since COUP observations are much more sensitive than Chandra observations in our sample, we also truncated the COUP sample at $\text{Log } L_X > 28.59$ corresponding to the lowest L_X of our sample. This prevents a comparison of inhomogeneous observations in terms of sensitivity limit. Making a list with the ONC sources and completing it with our HAEBE stars give us a unique opportunity to directly compare the X-Ray luminosity distribution of different spectral type stars. To make our statistical comparison consistent, we use their uncorrected L_X . This should not affect the ensemble statistics.

The sources were sampled into 3 groups of stellar objects: 1) Group I earlier than B3, 2) Group II intermediate mass stars, HAEBE, of spectral type B3-F5, and 3) Group III TTS, spectral type later than F5. We chose to use the spectral type to make different groups instead of the mass since the spectral type is often better known. However, we checked the known masses of Group III sources (or TTS) and found that their masses $\lesssim 3M_\odot$ are consistent with TTS.

Figure 7 shows the X-Ray luminosity variation with the spectral type. In Group I, the X-Ray luminosity is very scattered, $\sigma_{\text{Log}L_X} = 1.26$, around the mean value $\text{Log } L_X = 30.74$. Group II sources are less scattered, $\sigma_{\text{Log}L_X} = 0.82$, and have a slightly lower mean value $\text{Log } L_X = 30.1$. We also note in Group II that the L_X range of our sources is similar to the range of intermediate-mass stars from the COUP observations. There is no apparent dependence of L_X with spectral type in both Group I and II. On the other hand, Group III shows a slight dependence of the luminosity with spectral type. It decreases with the spectral type. The luminosity mean value is $\text{Log } L_X = 29.76$, smaller than in Group I and slightly smaller than in Group II. Figure 8 shows the L_X cumulative distribution function of TTS (Group III), Herbig Ae, Herbig Be, and HAEBE (Group II) samples. The L_X distribution for Group III follows a nearly uniform distribution. Herbig Ae's curve mostly resembles Group III's; but Group III's curve has a more extended tail toward lower L_X . Clearly the Herbig Be distribution is very different from the others. This is expected due to the very large scattered L_X (see Figure 7).

TTS' X-Ray luminosity shows some dependence on spectral type while the other groups do not. The detected X-Rays of the HAEBE stars may have a different origin than TTS companion, or the HAEBE stars do not emit in the X-Rays but have similar X-Ray emitting companions, hence an almost constant L_X . Nevertheless, some single HAEBEs have already shown intrinsic X-Ray emission (e.g. Swartz et al. 2005). Thus, the detected L_X may be a sum of the emission from the Herbig source and a possible companion's emission.

4.2. Statistical comparison

To quantify our finding, we use a Kolmogorov-Smirnov (K-S) (e.g. Press et al. 1993) and the Wilcoxon rank-sumtest (WRS) tests (Lehmann 1975) to test the L_X distributions. To check the robustness of this statistical comparison, we split randomly the largest sample, Group III, into 2 sub-Groups (test1 in Table 5). We find that the two sub-Groups derive from the same distribution, with a confidence level higher than 99.99% (K-S) and 95% (WRS). This shows that our strategy is effective.

The results are presented in Table 5. The two tests (K-S and WRS) provide a consistent variation of the probability, WRS probabilities are lower, which may be due to the difference of the median values of L_X in each Group.

4.3. Discussion

We can rule out the hypothesis that X-Rays detected toward Herbig systems (Group II) are from TTS companions with an 80% confidence level. Furthermore, we can not reject the hypothesis that Herbig Ae stars and TTS X-Rays derive from a same distribution. The probability, 12%, that Herbig Ae stars' X-Rays having a different parent distribution than TTS is much lower than the entire Herbig stars ensemble. This may be due to the fact that the process generating the X-Rays in the Herbig Ae stars is similar to the TTS's. In the same way, it was already proposed that late Herbig Ae stars may have an outer convective zone that supports the magnetic activity, similar but quite thinner than TTS' (e.g. Skinner et al. 2004). Herbig stars and OB stars (Group I) have a same parent distribution at a 55% confidence level. This may be due to a similar origin of the X-Rays, magnetic activity caused by a fossil magnetic field from the parent molecular cloud. This may be the case for at least the more massive Herbig Be stars, which have a relatively different L_X distribution than the Herbig Ae stars (see §4.2), and evolve faster than the Herbig Ae stars (Natta et al. 2000). It is important to note that the uncertainties of the source spectral type will affect

the group selection, particularly at the edges around F5 or B2. When placing sources in the group, we compared their masses (e.g. Getman et al. 2005b) before placing them in the respective group. However, this is not a large effect on our statistical tests as the key parameter is the overall distribution of the L_X over the group, not the exact placement in the group. Stelzer et al. (2006) reported that the X-Ray emission from HAEBE stars was qualitatively more similar to TTS in ONC than main sequence OB stars. However, this was based on a plot of L_X versus kT and was not quantified.

5. Summary

The relevance of our X-Ray study of HAEBE stars is due to our large sample with a somewhat arbitrary source selection; more than half of the sources were serendipitous observations. In addition, this is the first time where such a large sample of HAEBE stars are investigated in X-Rays with the high resolution of Chandra. The main results of this study are:

1) Out of 22 HAEBE sources, 14 have been detected in X-Rays, about 64%. The Herbig Ae stars have a higher rate of detection compared to the Herbig Be stars. The luminosity ranges between $\text{Log } L_X = 30\text{-}31$ (ergs/s). This is higher than TTS but overlaps the TTS L_X range. We report the first detection of V361 Ori and the first detections of AB Aur and V372 Ori with Chandra.

2) Although, the wind kinetic energy is strong enough to produce the detected L_X , the estimated temperatures are relatively high to be generated by such low-velocities. This shows that the wind shock model does not appear to generate the observed X-Rays, but one needs to be careful as this statement is based on only a few sources. More investigation including more sources with known v_{wind} need to be done to confirm this. Nevertheless, HD 104237 has a relatively high wind velocity. Its X-Ray emission can be partially or fully due to the kinetic L_{kin} .

3) Comparing the X-Ray emission to the stellar parameters: i) A luminosity ratio $\text{Log } L_X/L_{bol} = -5.62 \pm 1.18$ is lower than the typical TTS's ratio; ii) There is no correlation with the rotational period P_{rot} , which excludes the possibility of a solar-like dynamo effects to produce the X-Rays for the Herbig stars for which we know $v \sin i$; iii) We deduced a nearly linear correlation between the continuum radio emission at $\lambda=3.6$ cm and L_X toward Herbig Ae sources, with known $L_{3.6cm}$. Thus, suggesting that the emission does not depend on a companion.

4) The results of §4 show that HAEBE stars' X-Ray emission being from an unresolved

TTS companion can be ruled out at an 80% confidence level using the K-S test on the L_X distribution. In addition, the results show that the X-Ray emission of HAEBE stars is different than OB stars with only a 45% confidence level.

Overall, we suggest that the X-Rays are intrinsic to the HAEBE stars. In that case, they must have stellar magnetic activity. This is likely due to the remnant magnetic field after the collapse (Tassis & Mouschovias 2004; Montmerle et al. 2005). Indeed Wade et al. (2007) using spectropolarimeter observations reported the measurement of a magnetic field toward HAEBE stars. The existence of circumstellar disks toward HAEBE systems have been confirmed observationally in the last few years (e.g. Natta et al. 2000). Star-disk magnetic interaction can be an appropriate explanation of the X-Ray origin (e.g. Montmerle et al. 2000).

We are grateful to the anonymous referee for the several valuable suggestions to improve the paper. We thank Thierry Montmerle for his helpful comments on the paper. We acknowledge support from the Laboratory for Astronomical Imaging at the University of Illinois and NSF AST 0228953. We would like to thank Alastair Sanderson and Rosa Williams for their interesting comments. We would like to thank Alessandro Gardini for the several discussions on physical processes in the X-Ray.

REFERENCES

- Arnaud, K. A. 1996, in ASP Conf. Ser. 101: Astronomical Data Analysis Software and Systems V, edited by G. H. Jacoby, & J. Barnes, 17
- Baines, D., Oudmaijer, R. D., Porter, J. M., & Pozzo, M. 2006, MNRAS, 367, 737. [astro-ph/0512534](#)
- Berghoefer, T. W., Schmitt, J. H. M. M., Danner, R., & Cassinelli, J. P. 1997, A&A, 322, 167
- Damiani, F., Micela, G., Sciortino, S., & Harnden, F. R. 1994, ApJ, 436, 807
- Feigelson, E., Townsley, L., Güdel, M., & Stassun, K. 2007, in Protostars and Planets V, edited by B. Reipurth, D. Jewitt, & K. Keil, 313
- Feigelson, E. D., Lawson, W. A., & Garmire, G. P. 2003, ApJ, 599, 1207
- Feigelson, E. D., Broos, P., Gaffney, J. A., III, Garmire, G., Hillenbrand, L. A., Pravdo, S. H., Townsley, L., & Tsuboi, Y. 2002, ApJ, 574, 258. [astro-ph/0203316](#)

- Feigelson, E. D., & Montmerle, T. 1999, *ARA&A*, 37, 363
- Forbrich, J., Preibisch, T., & Menten, K. M. 2006, *A&A*, 446, 155
- Fuente, A., Martín-Pintado, J., Bachiller, R., Rodríguez-Franco, A., & Palla, F. 2002, *A&A*, 387, 977
- Fuente, A., Rodríguez-Franco, A., Testi, L., Natta, A., Bachiller, R., & Neri, R. 2003, *ApJ*, 598, L39
- Gagne, M., Caillault, J.-P., & Stauffer, J. R. 1995, *ApJ*, 445, 280
- Getman, K. V., Feigelson, E. D., Grosso, N., McCaughrean, M. J., Micela, G., Broos, P., Garmire, G., & Townsley, L. 2005a, *ApJS*
- Getman, K. V., Flaccomio, E., Broos, P. S., Grosso, N., Tsujimoto, M., Townsley, L., Garmire, G. P., Kastner, J., Li, J., Harnden, F. R., Wolk, S., Murray, S. S., Lada, C. J., Muench, A. A., McCaughrean, M. J., Meeus, G., Damiani, F., Micela, G., Sciortino, S., Bally, J., Hillenbrand, L. A., Herbst, W., Preibisch, T., & Feigelson, E. D. 2005b, *ApJS*
- Güdel, M. 2002, *ARA&A*, 40, 217. [astro-ph/0206436](#)
- Güdel, M. 2007, *Memorie della Societa Astronomica Italiana*, 78, 422
- Hamaguchi, K., Yamauchi, S., & Koyama, K. 2005, *ApJ*, 618, 360
- Hamidouche, M., Looney, L. W., & Mundy, L. G. 2006, *ApJ*, 651, 321. [astro-ph/0607232](#)
- Herbig, G. H. 1960, *ApJS*, 4, 337
- Hillenbrand, L. A., Strom, S. E., Vrba, F. J., & Keene, J. 1992, *ApJ*, 397, 613
- Isobe, T., Feigelson, E. D., Nelson, P. I. 1986, *ApJ*, 306, 490
- Kaastra, J. S., & Mewe, R. 2000, in *Atomic Data Needs for X-ray Astronomy*, p. 161, edited by M. A. Bautista, T. R. Kallman, & A. K. Pradhan, 161
- Kraft, R. P., Burrows, D. N., & Nousek, J. A. 1991, *ApJ*, 374, 344
- Lehmann, E. L. 1975, in *Nonparametrics: Statistical methods based on ranks*, edited by N. Y. McGraw-Hill
- Malfait, K., Bogaert, E., & Waelkens, C. 1998, *A&A*, 331, 211

- Mannings, V., & Sargent, A. I. 1997, *ApJ*, 490, 792
- Montmerle, T., Grosso, N., Tsuboi, Y., & Koyama, K. 2000, *ApJ*, 532, 1097
- Montmerle, T., Wade, G., Landstreet, J., Mènard, F., Grosso, N., & Feigelson, E. D. 2005, in *Protostars and Planets V*, Proceedings of the Conference held October 24-28, 2005, in Hilton Waikoloa Village, Hawai'i. LPI Contribution No. 1286., p.8112, 8112
- Mora, A., Merín, B., Solano, E., Montesinos, B., de Winter, D., Eiroa, C., Ferlet, R., Grady, C. A., Davies, J. K., Miranda, L. F., Oudmaijer, R. D., Palacios, J., Quirrenbach, A., Harris, A. W., Rauer, H., Cameron, A., Deeg, H. J., Garzón, F., Penny, A., Schneider, J., Tsapras, Y., & Wesseliuss, P. R. 2001, *A&A*, 378, 116
- Natta, A., Grinin, V., & Mannings, V. 2000, *Protostars and Planets IV*, 559
- Natta, A., Testi, L., Neri, R., Shepherd, D. S., & Wilner, D. J. 2004, *A&A*, 416, 179. [astro-ph/0311624](#)
- Pallavicini, R., Golub, L., Rosner, R., Vaiana, G. S., Ayres, T., & Linsky, J. L. 1981, *ApJ*, 248, 279
- Preibisch, T. 2007, *Memorie della Societa Astronomica Italiana*, 78, 332
- Press, W. H., Teukolsky, S. A., Vetterling, W. T., Flannery, B. P., Lloyd, C., & Rees, P. 1993, *Numerical recipes in Fortran: the art of scientific computing* / Cambridge U Press
- Rodríguez, L. F., Zapata, L., & Ho, P. T. P. 2007, *Revista Mexicana de Astronomia y Astrofisica*, 43, 149. [astro-ph/0611754](#)
- Skinner, S. L., Brown, A., & Stewart, R. T. 1993, *ApJS*, 87, 217
- Skinner, S. L., Güdel, M., Audard, M., & Smith, K. 2004, *ApJ*, 614, 221
- Stassun, K. G., Ardila, D. R., Barsony, M., Basri, G., & Mathieu, R. D. 2004, *AJ*, 127, 3537. [astro-ph/0403159](#)
- Stauffer, J. R., Caillault, J.-P., Gagne, M., Prosser, C. F., & Hartmann, L. W. 1994, *ApJS*, 91, 625
- Stelzer, B., Micela, G., Hamaguchi, K., & Schmitt, J. H. M. M. 2006, *A&A*, 457, 223. [astro-ph/0605590](#)

- Swartz, D. A., Drake, J. J., Elsner, R. F., Ghosh, K. K., Grady, C. A., Wassell, E., Woodgate, B. E., & Kimble, R. A. 2005, *ApJ*, 628, 811
- Tassis, K., & Mouschovias, T. C. 2004, *ApJ*, 616, 283
- Thé, P. S., de Winter, D., & Perez, M. R. 1994, *A&AS*, 104, 315
- Tokovinin, A., Thomas, S., Sterzik, M., & Udry, S. 2006, *A&A*, 450, 681. [astro-ph/0601518](#)
- van den Ancker, M. E., Bouwman, J., Wesselius, P. R., Waters, L. B. F. M., Dougherty, S. M., & van Dishoeck, E. F. 2000, *A&A*, 357, 325
- van den Ancker, M. E., de Winter, D., & Tjin A Djie, H. R. E. 1998, *A&A*, 330, 145
- Wade, G. A., Bagnulo, S., Drouin, D., Landstreet, J. D., & Monin, D. 2007, *MNRAS*, 376, 1145
- Zinnecker, H., & Preibisch, T. 1994, *A&A*, 292, 152

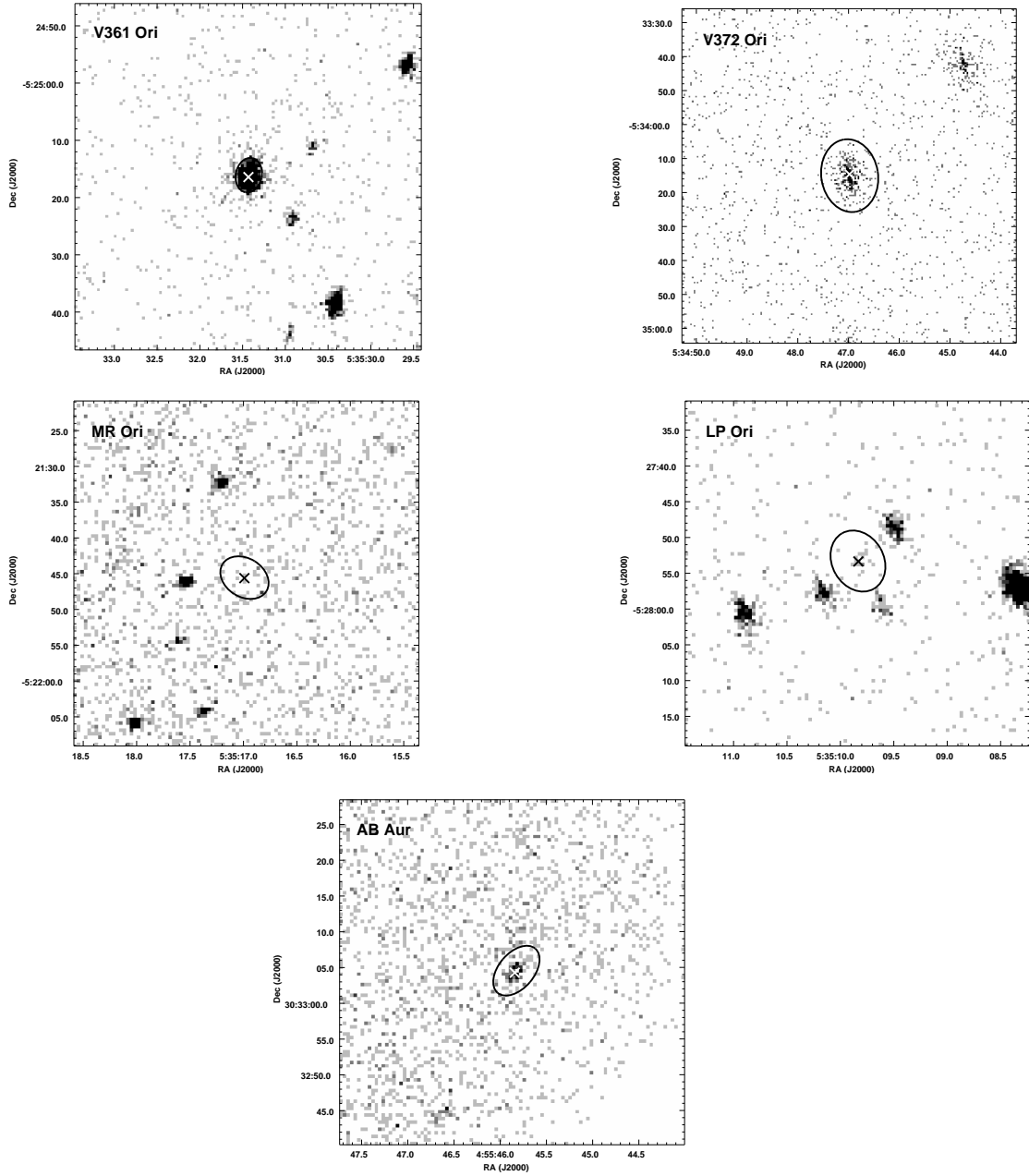


Fig. 1.— Maps of the five new observed Herbig sources with Chandra (§3.1). V361 Ori, V372 Ori, and AB Aur are detected and MR Ori and LP Ori are not detected (Table 3). The ellipses mark the PSF and the crosses the optical positions of the sources.

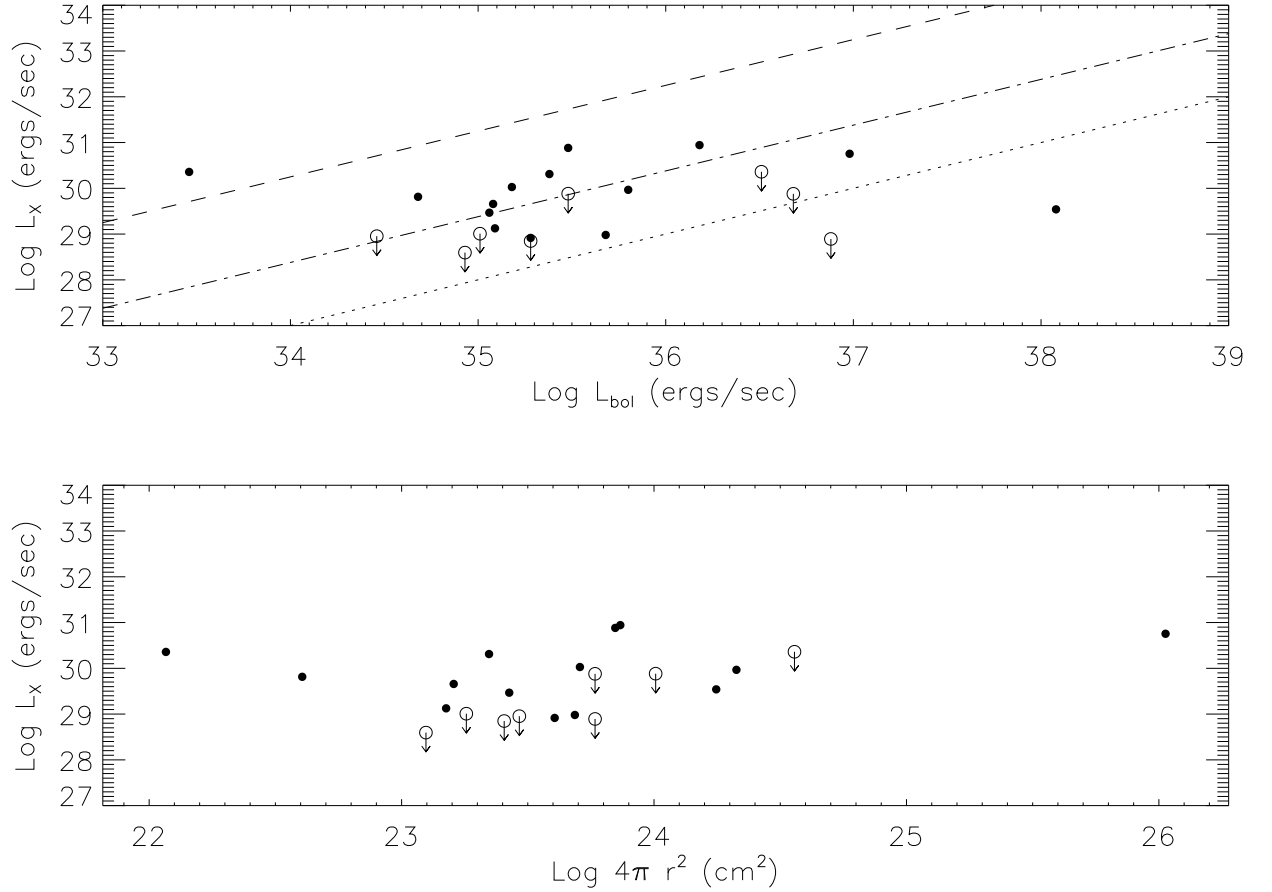


Fig. 2.— *Top*: X-Ray luminosity $\text{Log } L_X$ of detected and non-detected sources versus $\text{Log } L_{bol}$. For non-detected sources we give the upper limits, marked with the down pointing arrows. The straight lines correspond to $\text{Log } (L_X/L_{bol}) = -3.75$ (dashed), -5.62 (dash-dot), and -7.0 (dots). *Bottom*: $\text{Log } L_X$ versus the stellar surface area.

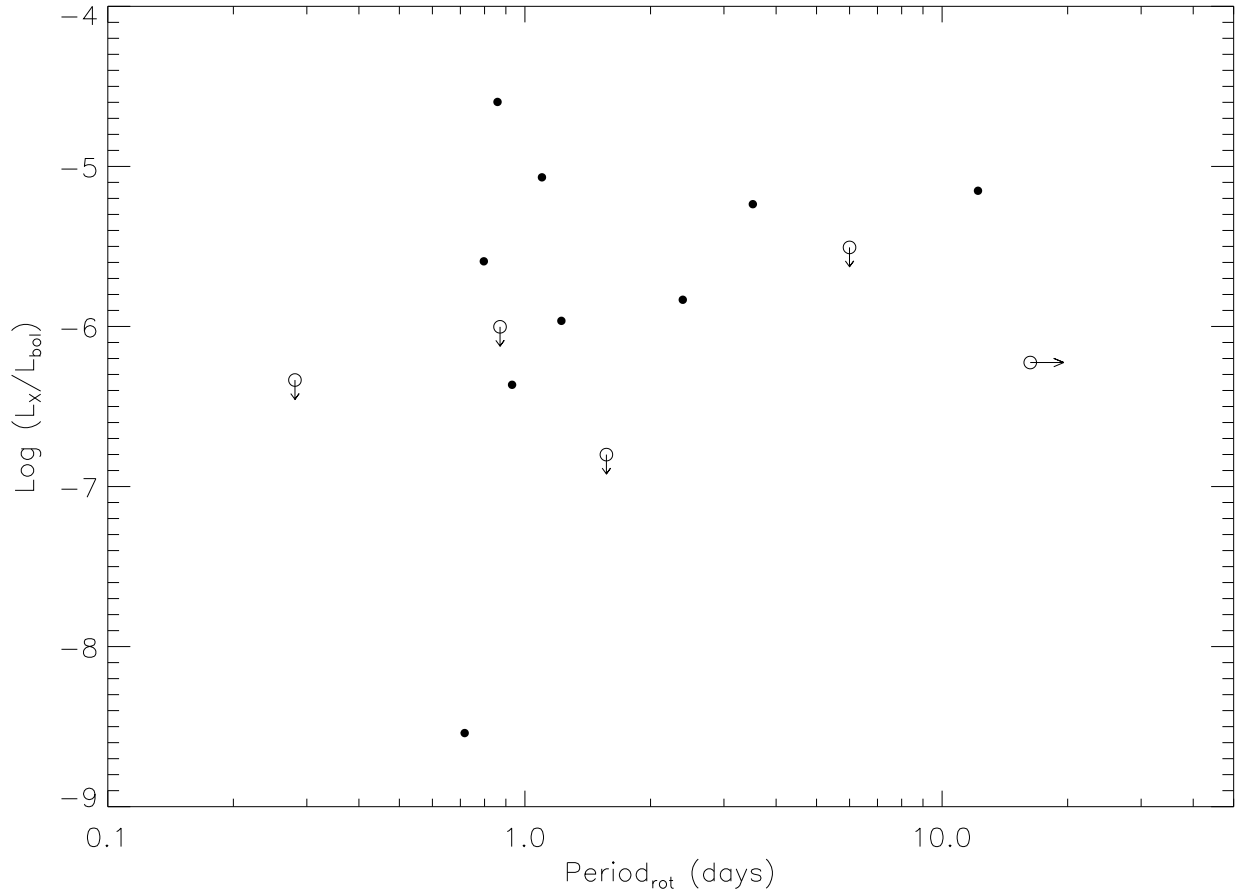


Fig. 3.— The luminosity ratio $\text{Log } L_X/L_{bol}$ versus the rotational period of the stars with known $v \sin i$. The down pointing arrows mark the upper limits of the luminosity ratio. The right pointing arrow marks the lower limit of the rotational period.

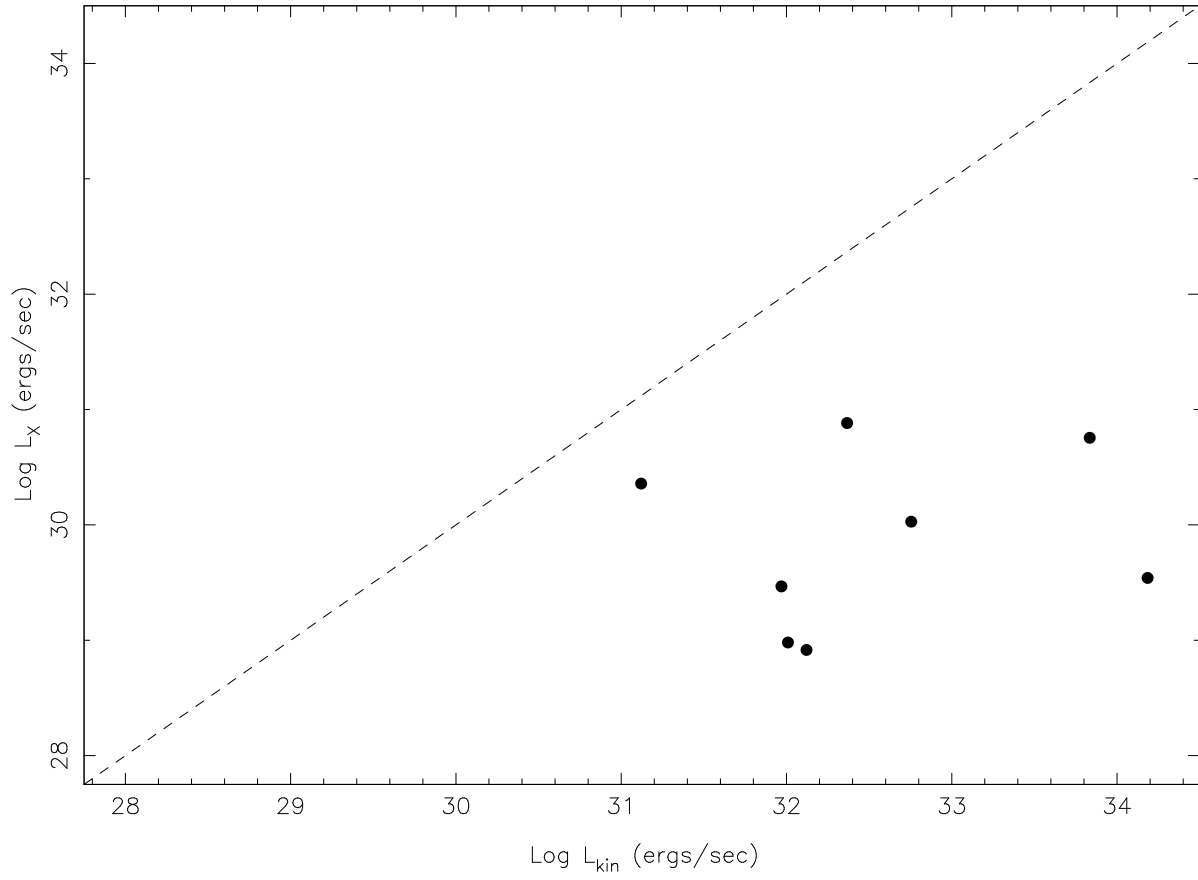


Fig. 4.— $\text{Log } L_X$ versus wind $\text{Log } L_{kin}$; the straight line corresponds to $L_X = L_{kin}$.

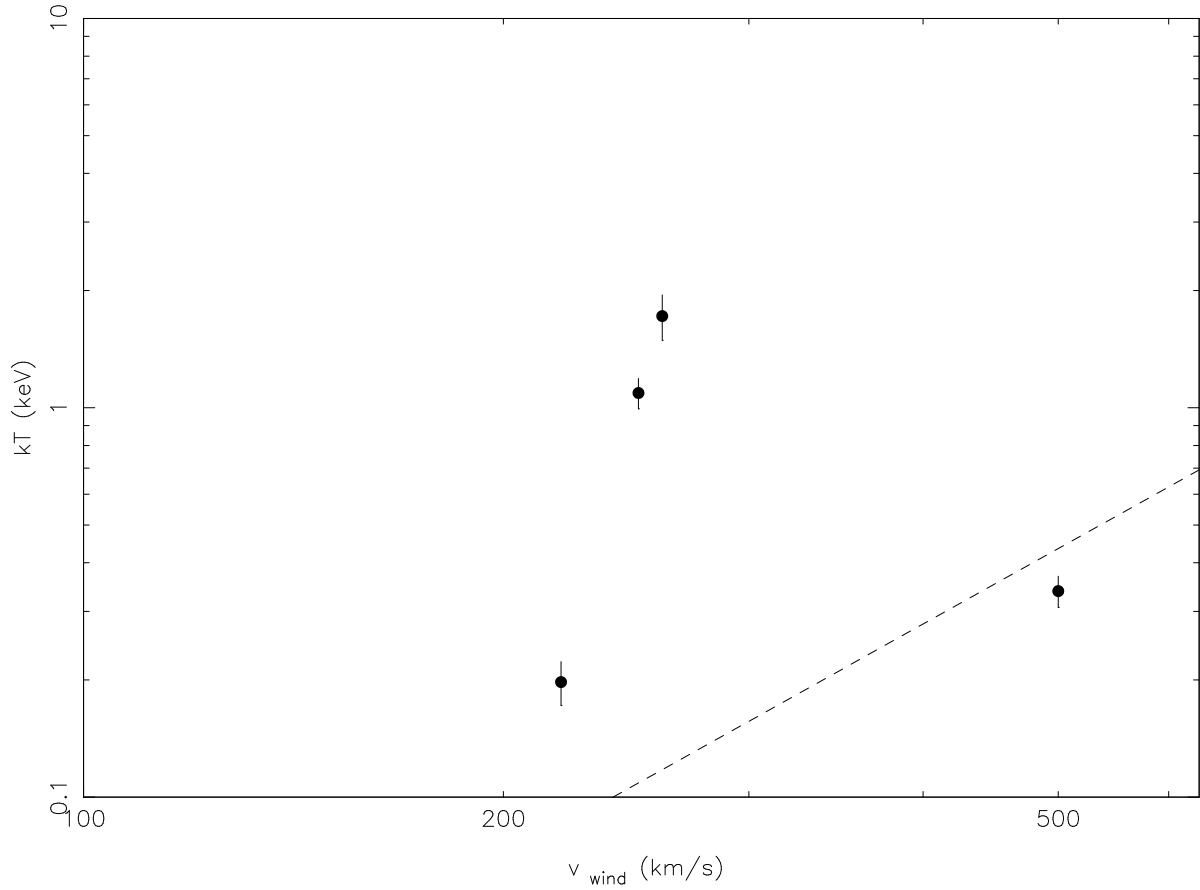


Fig. 5.— Plasma temperature kT versus wind velocity v_{wind} ; the straight line is deduced from the wind kinetic energy $kT = 1/3(\frac{1}{2}m_p v_{wind}^2)$, where m_p is the proton mass. HD 104237 is the source below the dashed line.

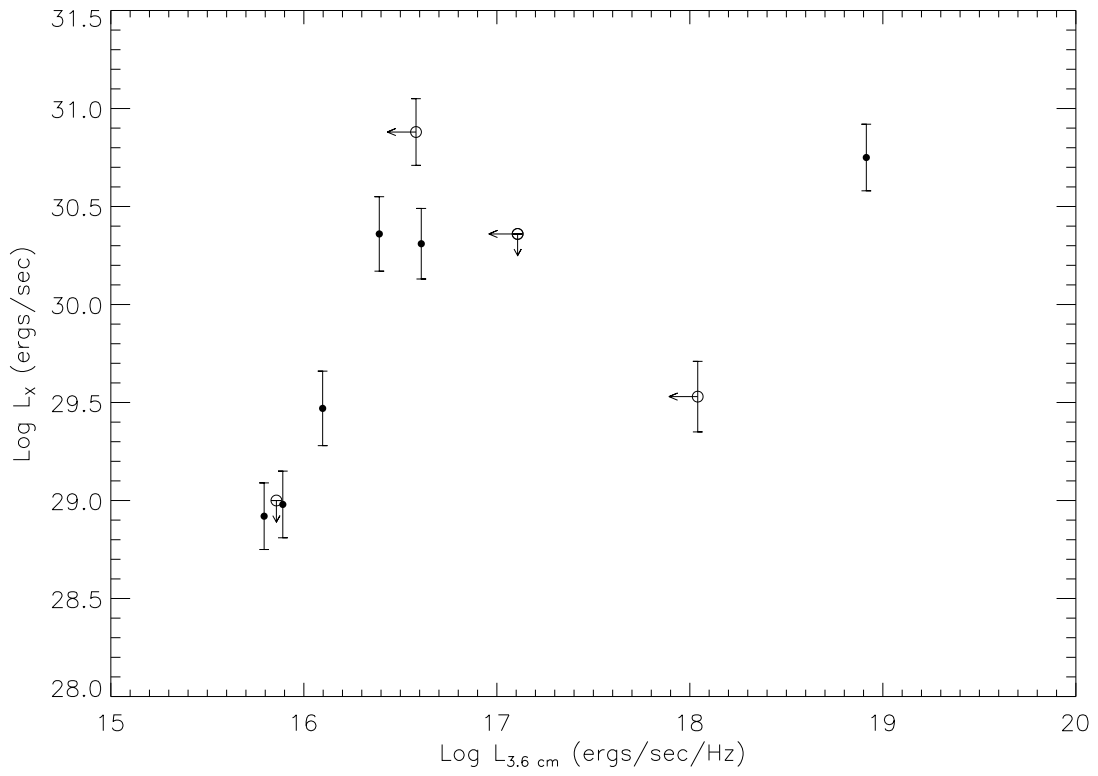


Fig. 6.— Variation of $\text{Log } L_X$ vs. radio $\text{Log } L_{3.6 \text{ cm}}$. The down pointing arrows mark the upper limits L_X . The left pointing arrows mark the upper limit of $L_{3.6 \text{ cm}}$.

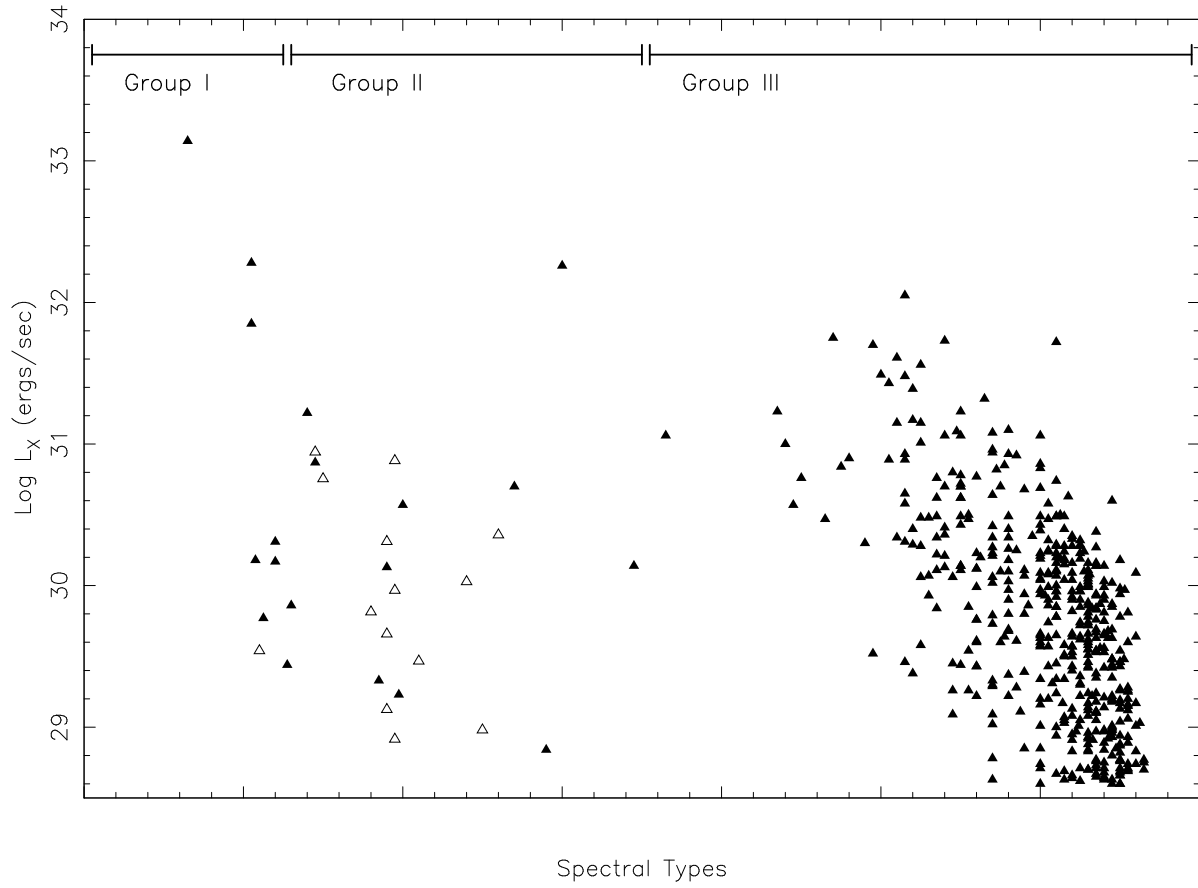


Fig. 7.— X-Ray luminosity from Chandra observations variation with the spectral type: *triangles* only the detected HAEBE data (Table 3) and *filled-triangles* COUP observations.

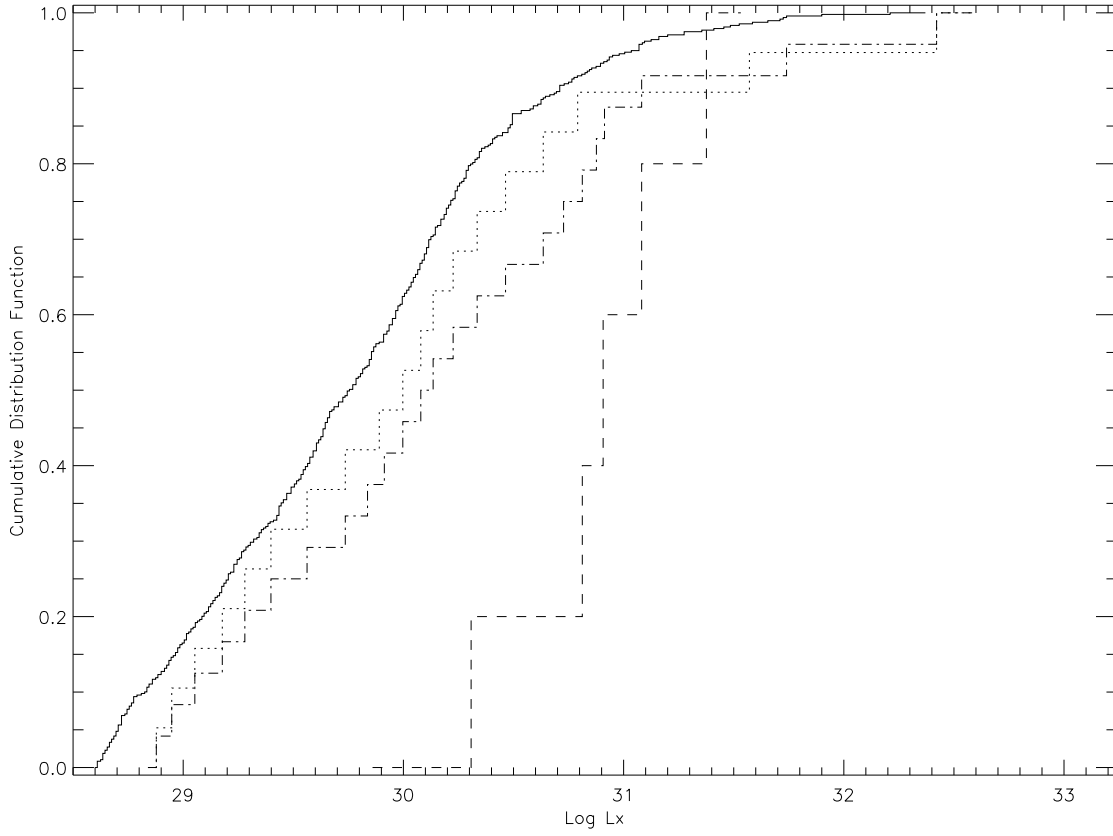


Fig. 8.— L_X Cumulative distribution function from Figure 7 of different samples: TTS (solid line), HAEBE (dash-dot line), Herbig Ae stars (dot line), and Herbig Be stars (dashed line).

Table 1. The physical parameters of the 22 Herbig AeBe stars.

Object	Spectral ^a Type	Distance ^a (pc)	Log L_{bol} ^{a,b} ($ergs\ s^{-1}$)	$S_{3.6cm}$ ^d (mJy)	Log T_{eff} ^{a,b} (K)	$v_{rot}\ sin\ i$ ^b ($km\ s^{-1}$)	v_{wind} ^{a,b} ($km\ s^{-1}$)	RA ^{a,b,c} (J2000)	DEC ^{a,b,c} (J2000)
MWC 297	B1Ve	250	38.08	<8.78	4.52	380	350	18 27 39.6	-03 49 52
LP Ori	B2	460	36.68	...	4.29	100	...	05 35 09.83	-05 27 53.33
HD 147889	B2	140	36.88	...	4.34	16 25 24.31	-24 27 56.56
V361 Ori	B4/5	460	36.18	...	4.14	50	...	05 35 31.43	-05 25 16.40
Z CMa	B5	1150	36.98	3.1	3.80	<130	500	07 03 43.16	-11 33 06.20
Lkh α 25	B7	800	36.51	<0.10	4.05	...	340	06 40 44.56	+09 48 02.2
BD+30 549	B8V	390	34.68	...	4.08	03 29 19.77	+31 24 57.04
R CrA	A5II	130	35.68	0.23	4.06	...	150	19 01 53.65	-36 57 07.62
V380 Ori	B8/A1	460	35.48	<0.09	3.97	200	260	05 36 25.43	-06 42 57.70
HD 97300	B9V	188	35.08	...	4.03	11 09 50.01	-76 36 47.72
HD 100546	B9V	103 \pm 7	35.09	...	4.04	65 \pm 5	...	11 33 25.44	-70 11 41.23
HD 176386	B9	130	35.28	...	4.03	19 01 38.93	-36 53 26.54
HD 141569	B9.5	99 $^{+9}_{-8}$	34.93	...	4.02	258 \pm 17	...	15 49 57.74	-03 55 16.36
AB Aur	B9/A0V	144 $^{+23}_{-17}$	35.28	0.15	3.98	140	225	04 55 45.84	+30 33 04.29
V372 Ori	B9.5V	460	35.8	...	3.93	125	...	05 34 46.98	-05 34 14.60
HD 150193	A2IV	150 $^{+50}_{-30}$	35.01	0.16	4	100	130	16 40 17.92	-23 53 45.18
HD 163296	A1	122 $^{+17}_{-13}$	35.06	0.42	3.97	133 \pm 6	220	17 56 21.28	-21 57 21.88
MR Ori	A2V	460	35.48	...	3.93	05 35 16.99	-05 21 45.6
TY CrA	B9	130	35.38	1.2	4.07	10	...	19 01 40.83	-36 52 33.88
Elias 3-1	A6	160	33.46	0.48	3.91	...	250	04 18 40.60	+28 19 16.7
HD 104237	A4	116 $^{+8}_{-7}$	35.18	...	3.93	12 \pm 2	500	12 00 05.08	-78 11 34.56
AK Sco	F5IV	150 $^{+40}_{-30}$	34.46	...	3.81	18.5 \pm 1	...	16 54 44.84	-36 53 18.57

^aRef. Hillenbrand et al. (1992), Thé et al. (1994), Malfait et al. (1998), van den Ancker et al. (1998), Natta et al. (2000), Fuente et al. (2002), Hamaguchi et al. (2005).

^bRef. Damiani et al. (1994), Skinner et al. (1993), Mora et al. (2001).

^cRef. This research has made use of the SIMBAD database, operated at CDS, Strasbourg, France.

^dRef. $S_{3.6cm}$ are from Skinner et al. (1993), Forbrich et al. (2006), and Natta et al. (2004).

Table 2. Chandra observations.

Object	Observation ID	Date	Detector	Exposure Time (s)	Intended Target
MWC 297	1883	2001-09-21	ACIS-I	7731.518	Yes
LP Ori	3498	2003-01-21	ACIS-I	66811.9	No
HD 147889	618	2000-06-22	ACIS-I	3000	No
V361 Ori	3498	2003-01-21	ACIS-I	66811.9	No
Z CMa	3751	2003-12-07	ACIS-S	37872.4	Yes
Lkh α 25	2550	2002-02-09	ACIS-I	48755.2	No
BD+30 549	642	2000-07-12	ACIS-I	43907.2	No
R CrA	3499	2003-06-26	ACIS-I	37976.736	Yes
V 380 Ori	21	2000-10-08	ACIS-S	19610.0	No
HD 97300	1867	2001-07-02	ACIS-I	66992.318	No
HD 100546	3427	2002-02-04	ACIS-I	2662.4	Yes
HD 176386	3499	2003-06-26	ACIS-I	37976.736	No
HD 141569	981	2001-06-23	ACIS-I	2803.60	Yes
AB Aur	3755	2003-11-27	ACIS-S	99622.8	No
V372 Ori	2548	2002-09-06	ACIS-I	47414.0	No
HD 150193	982	2001-08-19	ACIS-I	2806.8	Yes
HD 163296	3733	2003-08-10	ACIS-S	19988.4	Yes
MR Ori	2568	2002-02-19	ACIS-S	46928.0	No
TY CrA	3499	2003-06-26	ACIS-I	37976.736	No
Elias 3-1	3364	2002-03-07	ACIS-S	17811.6	No
HD 104237	3428	2002-02-04	ACIS-I	2714.0	Yes
AK Sco	983	2001-08-19	ACIS-I	3002.0	Yes

Table 3. X-Ray Detection of Herbig AeBe stars.

Object ^a	S/N	Count Rate (cts/ks)	PSF	Log L_X ($ergs\ s^{-1}$)	Intended Target	Log L_X/L_{bol}	Detected
MWC 297	4.54	2.88±0.52	0.9	29.53±0.18	Yes	-8.54	Yes
<u>LP Ori</u>	0.78	< 0.027	0.9	< 29.87	No	< -6.8	No
HD 147889	1.28	< 0.62	0.9	< 28.89	No	< -7.98	No
<u>V361 Ori</u>	54.64	44.59±0.56	0.9	30.94±0.17	No	-5.24	Yes
Z CMa	6.33	1.08±0.15	0.9	30.75±0.17	Yes	-6.14	Yes
Lkh α 25	0.98	< 0.04	0.9	< 30.36	No	< -6.15	No
BD+30 549	4.92	1.05±0.13	0.6	29.81±0.16	No	-4.87	Yes
R CrA	10.73	3.04±0.18	0.9	28.98±0.17	Yes	-6.69	Yes
V380 Ori	30.49	47.36±1.08	0.9	30.88±0.17	No	-4.60	Yes
HD 97300	32.76	16.03±0.34	0.9	29.66±0.18	No	-5.4	Yes
HD 100546	5.90	13.11±1.96	0.9	29.13±0.18	Yes	-6.1	Yes
HD 176386	1.14	<0.05	0.9	< 28.84	No	< -6.43	No
HD 141569	1.26	< 0.66	0.9	< 28.59	Yes	< -6.33	No
<u>AB Aur</u>	5.28	0.59±0.13	0.55	28.92±0.17	No	-6.36	Yes
<u>V372 Ori</u>	17.55	6.43±0.28	0.9	29.97±0.17	No	-5.83	Yes
HD 150193	1.95	<1.4	0.5	< 29.00	Yes	< -6.00	No
HD 163296	34.28	53.70±1.18	0.9	29.47±0.19	Yes	-5.59	Yes
<u>MR Ori</u>	0.62	< 0.07	0.9	< 29.88	No	< -5.59	No
TY CrA	71.55	134.88±1.31	0.9	30.31±0.18	No	-5.07	Yes
Elias 3-1	39.87	89.26±1.40	0.9	30.36±0.19	No	-3.10	Yes
HD 104237	20.48	154.34±5.67	0.9	30.03±0.18	Yes	-5.15	Yes
AK Sco	1.31	< 0.63	0.9	< 28.95	Yes	< -5.50	No

^aThe underlined sources' observations are reported in this study for the first time (§3.1).

Table 4. X-ray parameters from the spectral analysis.

Object	Model	T ^a (keV)	$N_{H_2}(10^{22} \text{ cm}^{-2})$	χ_r^2 (dof) ^b
V361 Ori	2T	0.95,3.08	0.13±0.03	0.38(273)
V380 Ori	2T	1.12,2.31	0.15±0.07	0.44(121)
HD 97300	2T	0.86,2.91	0.31±0.15	0.17(310)
V372 Ori	1T	0.97	0.18±0.01	1.03(23)
HD 163296	1T	0.39	0.06±0.05	0.19(542)
TY CrA	2T	0.79,2.07	0.21±0.04	0.33(303)
Elias 3-1	1T	2.18	0.67±0.18	0.21(360)
HD 104237	1T	0.67	0.38±0.07	0.13(430)

^aFitted temperatures using one- or two-temperature MEKAL models, based on the best fit model or χ^2 .

^bReduced χ^2 level and the number of degrees of freedom in parentheses.

Table 5. K-S and WRS tests results of two samples being drawn from a same parent distribution.

Test	Datasets ^a	K-S test probability ^b (%)	WRS test probability ^b (%)
1 ^c	sub-Group III – sub-Group III	99.99	95
2	Group I – Group II	55	28
3	Group II – Group III	20	6
4	Group I – Group III	9	2
5	Herbig Ae – Group III	88	42

^aSee §4.1: Group I (<B3), Group II (B3-F5), Group III (> F5)

^bSmall values of the probability show that the distributions of the 2 datasets are significantly different.

^cSplitting randomly Group III in half to make 2 sub-Groups; taking then the tests on these 2 sub-Groups allows to check the robustness of our tests.